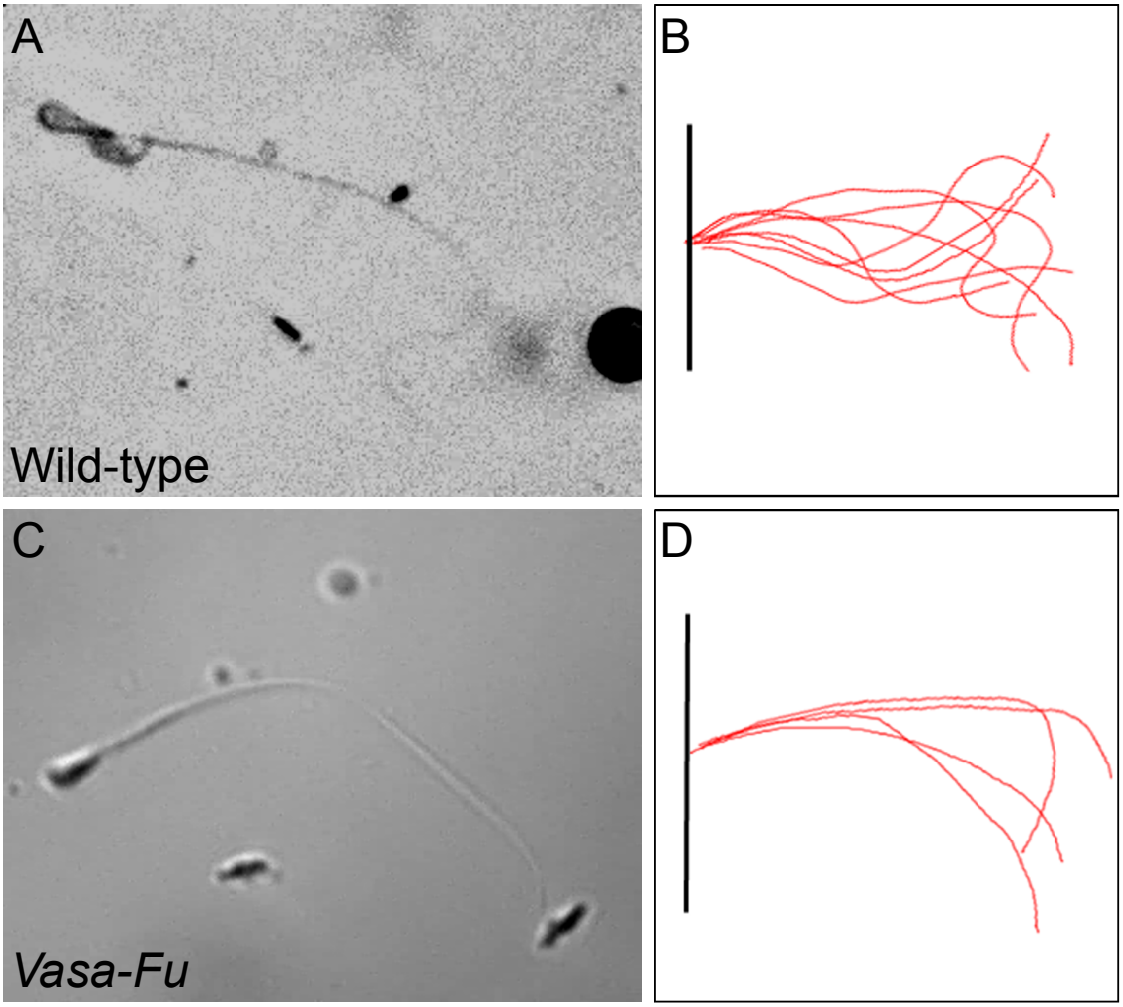

Fig. S1: *Vasa-Fu* sperm flagellum cannot propagate a waveform
(A) Still image of a capacitated wild-type mouse sperm from a movie clip; it was beating and bending of the flagellum was detected. (B) Traces of successive movements of the sperm flagellum (movie taken at approximately 3.2 frames per second (f.p.s.)). The wild-type flagellum initiated bending at the base of the head and propagated the wave through the tail at a high frequency and amplitude. (C) Still image of a motile *Vasa-Fu* sperm from a movie clip. (D) Traces of successive movements of the sperm flagellum (movie taken at approximately 2 f.p.s.). The *Fu*-deficient flagellum can barely initiate a bend and no wave was propagated. The sperm did not advance from its original location.

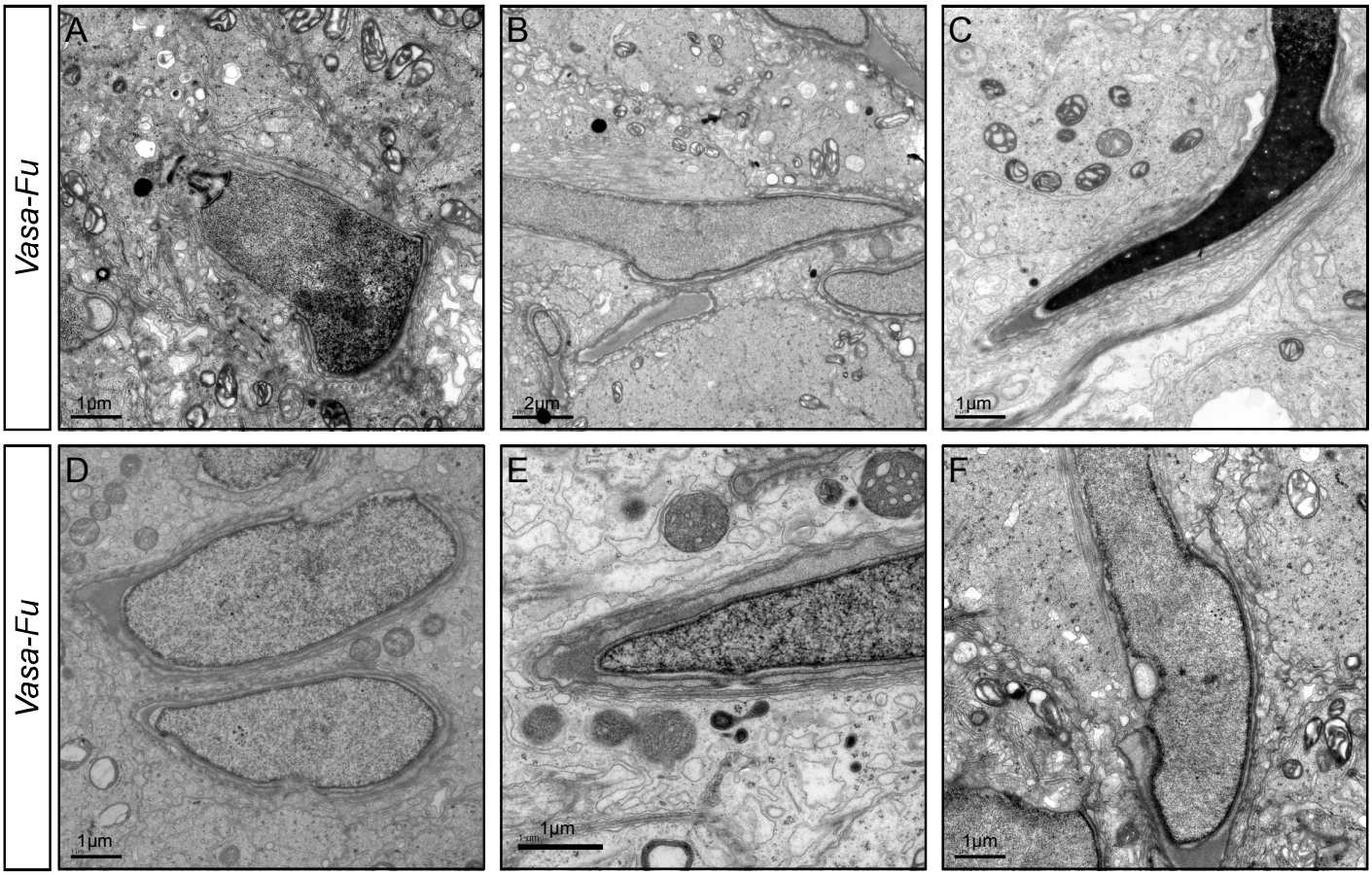

Fig. S2: *Vasa-Fu* spermatozoa frequently display abnormal nuclear head shaping and fragmentation of the acrosome-acroplaxome complex
(A-C) Transmission electron micrographs of elongating spermatids collected from the testes of *Vasa-Fu* adult mice. The nucleus was often excessively elongated and local constriction was also evident.
(D-F) Breaks in the acrosome-acroplaxsome membrane (D, E) or large vesicles (F) between the acrosome and the nuclear envelope were observed.

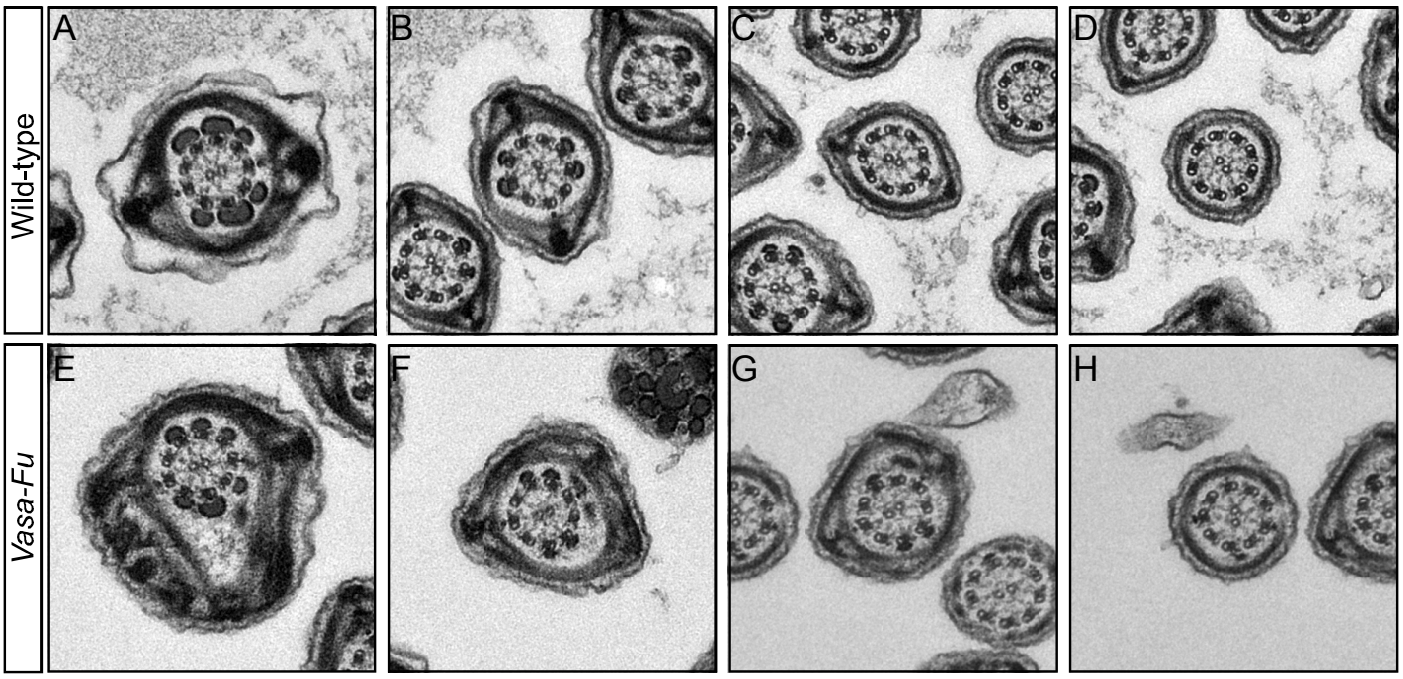

Fig. S3: *Vasa-Fu* sperm flagella from cauda epididymis have periaxonemal abnormalities
Transmission electron micrographs of sperm collected from the cauda epididymis of wild-type (A-D) and *Vasa-Fu* (E-H) adult mice. Sections from left to right showed proximal to distal progression through the principal piece. The fibrous sheath was often distorted in the principal piece of *Vasa-Fu* sperm and the presence of extra longitudinal columns was also observed.

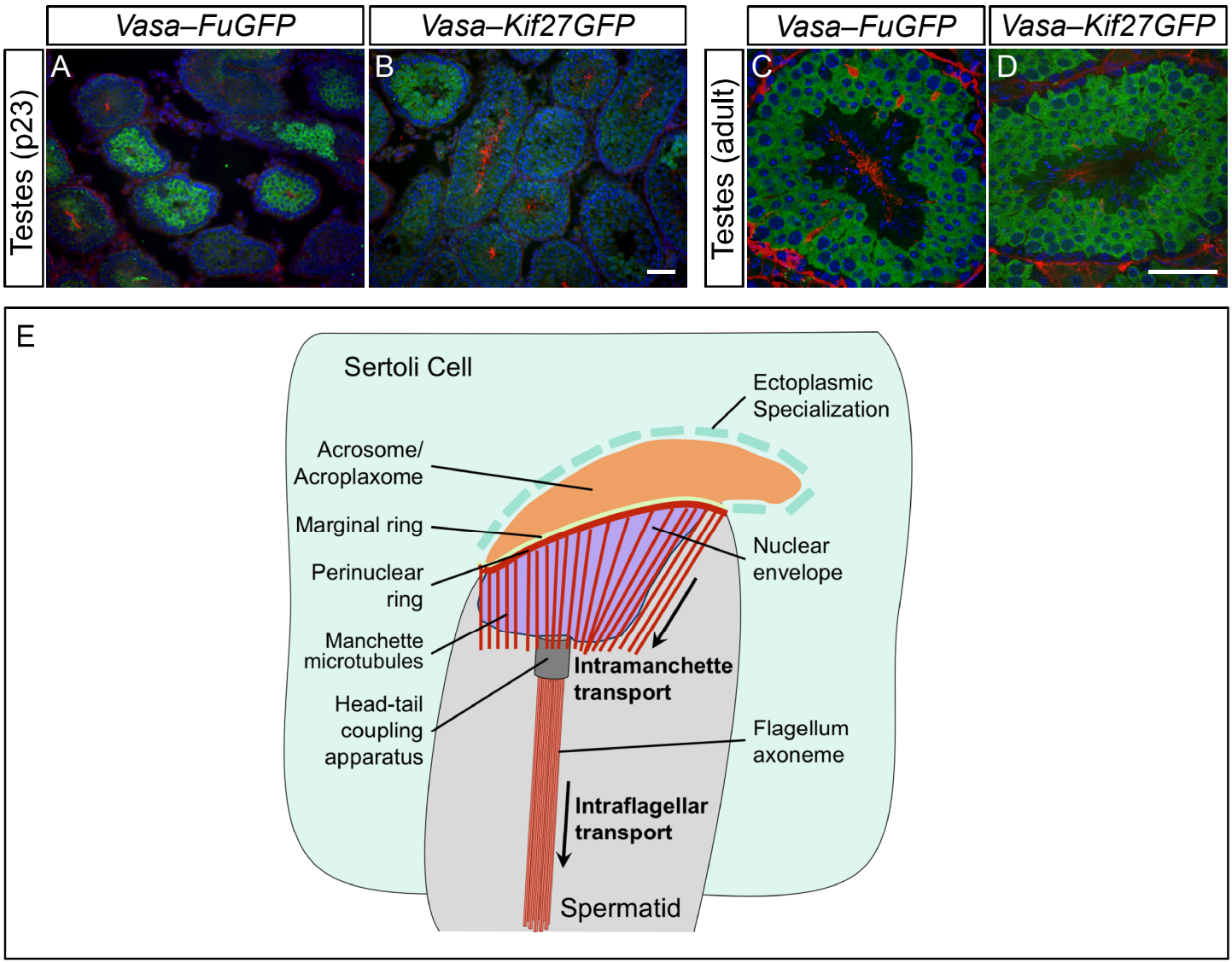

Fig. S4: FuGFP and Kif27GFP are detected in the germ cells of the testes
(A, B) Immunofluorescence of sections derived from *Vasa-FuGFP* and *Vasa-Kif27GFP* mice at postnatal (p) day 23 stained with anti-GFP (green), anti-acetylated tubulin (red) and DAPI (blue). GFP signal was restricted to the germ cells. (C, D) Immunofluorescence of testicular sections from adult *Vasa-FuGFP* and *Vasa-Kif27GFP* mice stained with anti-GFP (green). GFP signal was broadly detected in spermatocytes and spermatids, but its intensity drops precipitously in spermiating cells. Scale bar = 50 μm for A-B, C-D.
(E) Schematic diagram of the microtubule- and actin-based transport system in the elongating mouse spermatid. The Sertoli cell attaches to the spermatid through F-actin-containing ectoplasmic specializations (ES) and the F-actin bundles in the ES exert pressure on the spermatid head during the elongation of the nucleus. The acrosome cap of the spermatid is attached to the nuclear envelope (purple) through a keratin/F-actin plate called the acroplaxome. The marginal ring of the acroplaxome delineates the leading edge of the acrosome. During spermatid development, a transient manchette structure encloses the more distal part of the nucleus. The manchette appears during the acrosome phase (steps 8-14) and is believed to shape the nuclear head. It disappears by step 15 of spermiogenesis after which the spermatozoa shed its cytoplasmic material prior to spermiation (maturation phase). The perinuclear ring of the manchette and the adjacent marginal ring shrink in diameter and direct the shaping of the spermatid head. As the manchette and acrosome-acroplaxome shaped the nucleus, the perinuclear ring reaches the caudal end of the nucleus. Microtubule tracks extend from the perinuclear ring and it is hypothesized that this enables the transport of cargos (called intramanchette transport) from the nucleus to the cytoplasm and to the head-tail coupling apparatus and eventually the spermatid tail. Intramanchette transport (IMT) is analogous to intraflagellar transport (IFT) on the axoneme of the flagellum since they share similar components such as the molecular motors and IFT proteins.

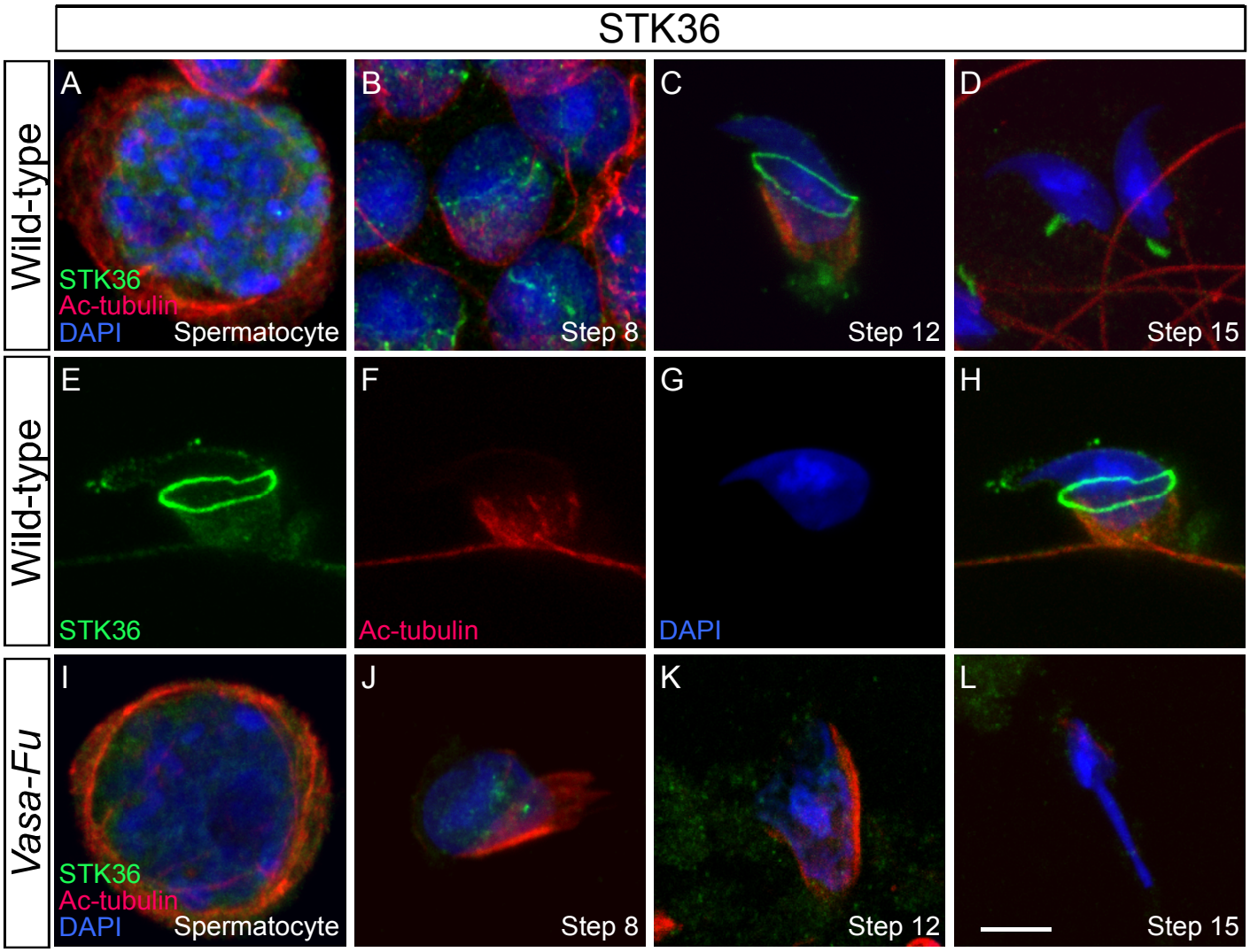

Fig. S5: STK36 antibody detects distribution of endogenous STK36 (Fu) in the developing spermatozoa
(A-H) Confocal immunofluorescence of testicular cells derived from wild-type adult mice. Cells were stained with antibodies against STK36 (green) and acetylated (Ac) tubulin (red). The nucleus was stained with DAPI (blue). STK36 signal was detected in the cytoplasm of spermatocytes (A), in the manchette of round spermatids (B), and in the perinuclear ring of round (B), elongating (C) and elongated spermatids (D). (E-H) An elongating spermatid (step 12/13) stained against STK36 antibody (green) showed localization of endogenous STK36 (Fu) to the perinuclear ring, the manchette and the acrosome-acroplaxome. STK36 signal was weaker in the manchette and the acrosome-acroplaxome complex. (I-L) Confocal immunofluorescence of testicular cells derived from *Vasa-Fu* adult mice and stained with STK36 antibodies. Only background signal was detected. Scale bar = 5 µm for A-L.

Stages of spermatid development: Golgi phase, steps 1-3 (formation of acrosome granules from Golgi-derived vesicles, beginning of tail formation); cap phase, steps 4-7 (formation of the acrosome cap from acrosome granules); acrosome phase, steps 8-14 (formation of the acrosome and manchette structures); maturation phase, steps 15-19 (midpiece formation, shrinkage of the cytoplasm and formation of the residual body).

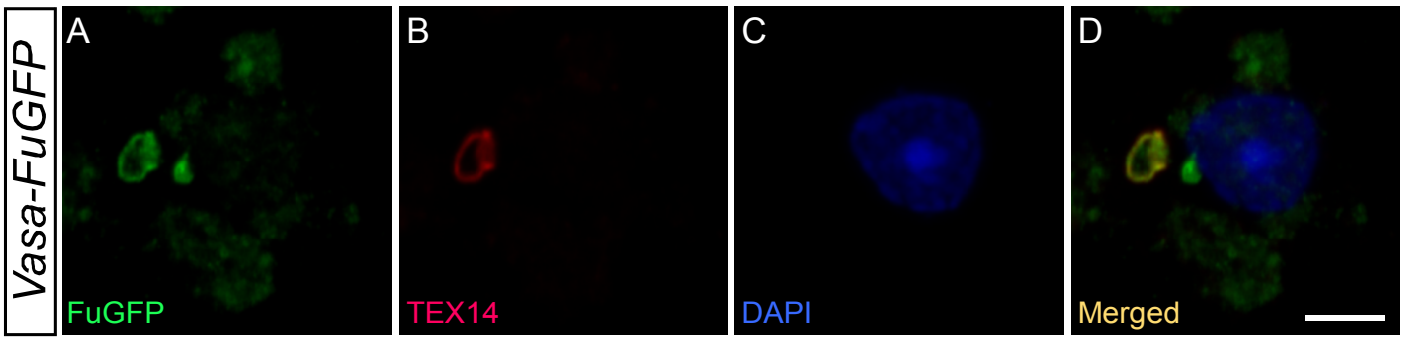

Fig. S6: FuGFP signal coincides with TEX14 antibody staining in the intercellular bridges of spermatids
(A-D) Confocal immunofluorescence of a step 7/8 round spermatid derived from *Vasa-FuGFP* adult mice. Spermatids were stained with antibodies against GFP (green) and TEX14 (red); the nucleus was stained with DAPI (blue). TEX14 is specific to the intercellular bridges in the developing spermatids. FuGFP staining coincided with that of TEX14, indicating that FuGFP localizes to the intercellular bridges of the developing spermatids. Scale bar = 5 μm for A-D.

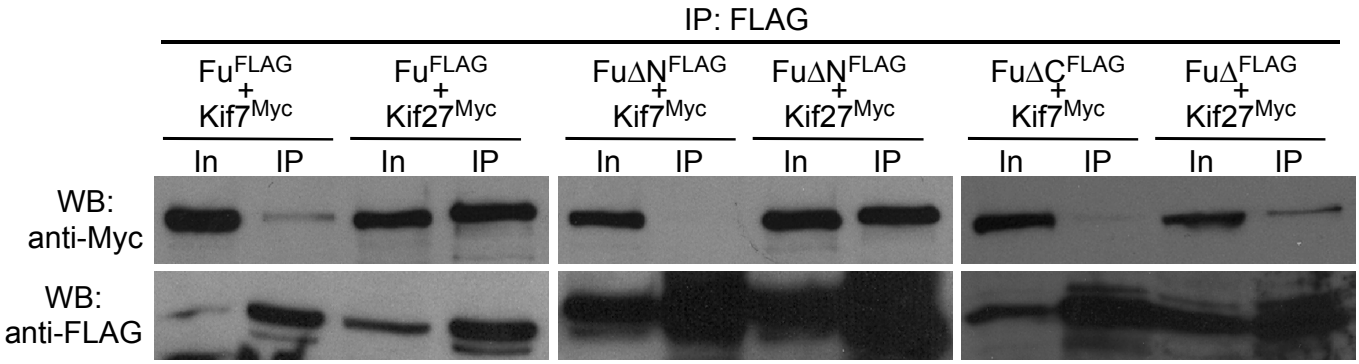

Fig. S7: The Fu regulatory domain interacts with Kif27
Western blot of immunoprecipitated Fu^{FLAG} and deletion mutants of Fu ($Fu\Delta N^{FLAG}$ and $Fu\Delta C^{FLAG}$) to test physical interactions between Fu and Kif27 using HEK293T cell lysates. $Kif27^{Myc}$ was pulled down from the cell lysate when Fu^{FLAG} or $Fu\Delta N^{FLAG}$ (lacking the N-terminal kinase domain) was immunoprecipitated. By contrast, $Kif27^{Myc}$ failed to be co-immunoprecipitated with $Fu\Delta C^{FLAG}$ that lacks the C-terminal regulatory domain. As controls, $Kif7^{Myc}$ failed to be pulled down by Fu or Fu deletion mutants. In, input; IP, immunoprecipitation; WB, Western blot.